CARBON 79 (2014) 493–499

Available at www.sciencedirect.com

ScienceDirect

journal homepage: www.elsevier.com/locate/carbon

Mesoporous zinc ferrite/graphene composites: Towards ultra-fast and stable anode for lithium-ion batteries

Xiayin Yao, Junhua Kong, Dan Zhou, Chenyang Zhao, Rui Zhou, Xuehong Lu *

School of Materials Science and Engineering, Nanyang Technological University, 50 Nanyang Avenue, Singapore 639798, Singapore

ARTICLE INFO

Article history:
Received 31 March 2014
Accepted 5 August 2014
Available online 12 August 2014

ABSTRACT

Mesoporous zinc ferrite ($ZnFe_2O_4$)/graphene composites are synthesized using a facile ambient-pressure method, i.e., co-precipitation of metal cations onto graphene oxide followed by solid state reaction to yield $ZnFe_2O_4$ nanoparticles anchored on reduced graphene oxide. The resultant $ZnFe_2O_4$/graphene composites have large specific surface area with mesopores, and the size of the $ZnFe_2O_4$ nanoparticles is less than 20 nm. When the composites are employed as an anode material for lithium-ion batteries, it exhibits superior electrochemical performances in term of high reversible capacity, good cyclic performance and excellent rate capability. Its reversible discharge capacities can be maintained at 870 mAh/g at 1.0 A/g for 100 cycles and consecutively 713 mAh/g at 2.0 A/g for another 100 cycles. Moreover, other graphene-based composites containing ferrites, such as cobalt ferrite and nickel ferrite, are also synthesized with this generic strategy which is promising for large-scale production of lithium-ion battery anode materials.

1. Introduction

Rechargeable lithium-ion batteries (LIBs) have been widely used as power sources for portable electronic products and are regarded as one of the leading candidates for powering hybrid electric or all-electric vehicles [1]. The major limitation of the currently used graphite anode in LIBs is that its theoretical capacity is only 372 mAh/g. In order to meet the increasing demand for higher energy and power density batteries, great efforts have been made to develop new anode materials, such as transitional metal oxides [2], oxysalts [3] and silicon [4–6]. Among these newly developed anode materials, zinc ferrite ($ZnFe_2O_4$) has been considered to be a promising candidate for LIB anodes because of its non-toxicity, being environmentally friendly, good structural stability and low cost [7]. It has been reported that each formula unit of $ZnFe_2O_4$ can react with nine Li ions, giving a theoretical specific capacity of about 1000.5 mAh/g [8,9]. However, $ZnFe_2O_4$ anode materials usually suffer from low rate capability resulting from poor electrical conductivity as well as kinetic limitations and poor cycling performance owing to large volume changes induced by electrode pulverization during repeated lithiation/delithiation processes. Generally, these problems could be alleviated by preparation of nano-structured electrodes with carbonaceous materials [10–13], which can buffer the volume expansion as well as increase the electrical conductivity.

Recently, graphene, a type of two-dimensional carbon nanomaterial with excellent conductivity and structural flexibility, has been used by researchers as the carbonaceous materials in LIB electrodes to improve their cycling stability

* *Corresponding author:* Fax: +65 6790 9081.
E-mail address: ASXHLu@ntu.edu.sg (X. Lu).
http://dx.doi.org/10.1016/j.carbon.2014.08.007
0008-6223/

and rate capability [14–16]. There is already some reported work on $ZnFe_2O_4$/graphene composites for LIBs [17–19] and photocatalysis applications [20–22]. A $ZnFe_2O_4$/graphene nanohybrid synthesized via a solvothermal route exhibits enhanced electrochemical properties when employed as anodes of LIBs [17]. Similarly, Fu and Wang [20] prepared $ZnFe_2O_4$/graphene composites via a hydrothermal method and investigated their photocatalytic activity for degradation of methylene blue under visible light. The results show that the photoactivity is significantly improved by combination of graphene and $ZnFe_2O_4$. However, so far the reported synthesis strategies for $ZnFe_2O_4$/graphene composites all involve high-pressure processes, which are not ideal for mass production of the composites for practical applications.

Very recently, metal oxide electrodes with mesoporous morphologies have been demonstrated to be beneficial to electrochemical performance of lithium-ion batteries as the nanometer-scale porosity allows easy electrolyte access to the electrode surfaces, facilitating charge transfer across the electrode/electrolyte interface, as well as accommodates the volume changes during Li-ion insertion/extraction [23,24]. Porous $ZnFe_2O_4$ nanostructures could be synthesized by thermal decomposition of oxalate precursor [25] or double hydroxide precursor at ambient pressure [26,27]. It is anticipated that the combination of mesoporous $ZnFe_2O_4$ with conductive graphene nanosheets would enhance electrical conductivity of the active material while ensuring good access of the electrolyte to the material surface, leading to significantly improved electrochemical performance.

In this work, we report a facile two-step strategy for synthesis of mesoporous $ZnFe_2O_4$/graphene composites as high-performance anode materials for LIBs. By this route, $ZnFe_2O_4$ nanoparticles with sizes of less than 20 nm can be simultaneously formed and anchored on the graphene nanosheets. Compared with the $ZnFe_2O_4$/graphene composites reported in literatures, the $ZnFe_2O_4$/graphene composites prepared in this work show a mesoporous structure with pore size of less than 10 nm and exhibit superior electrochemical performances in term of high reversible capacity, good cyclic performance and excellent rate capability. Moreover, this synthesis strategy contributes a generic route for large-scale production of binary transitional metal oxide/graphene composites that may be used for LIBs and many other applications.

2. Experimental

2.1. Synthesis of the mesoporous $ZnFe_2O_4$/graphene composites

All of the chemicals were analytical grade and used without further purification. The composites were synthesized through a two-step procedure, including the co-precipitation of metallic cations onto graphene oxide (GO) and solid state reaction in order to form mesoporous $ZnFe_2O_4$ as well as reduce GO to graphene. GO was synthesized from graphite powder (natural, −10 mesh, Alfa Aesar, 99.9%) according to a modified Hummers' method [28,29]. The concentration of the obtained homogeneous GO colloid suspension in water is about 2.5 mg/ml. To synthesize the composites, in a typical synthesis, 60 g of 2.5 mg/ml GO aqueous suspension was further diluted with 340 g deionized water, and then 10 ml ammonium hydroxide solution (Aldrich, 28.0–30.0%) was added with stirring in order to adjust the pH of the system to 10. After that, 180 ml aqueous solution containing 0.4 mmol of zinc sulfate heptahydrate (Aldrich, ⩾99.0%) and 0.8 mmol of iron sulfate heptahydrate (Aldrich, ⩾99.0%) were dropwise added to the above suspension at room temperature and further stirred for 6 h. The precipitate was collected by centrifuge and repeatedly washed with deionized water, and then freeze dried. Finally, the obtained precursor was calcinated by heating it to 600 °C at the rate of 5 °C min^{-1} and keeping at 600 °C for 2 h in argon atmosphere. $ZnFe_2O_4$ nanoparticles were also prepared under the same reaction conditions except in the absence of GO. Graphene nanosheets were obtained by carbonization of freeze-dried GO under 600 °C for 2 h in argon atmosphere.

2.2. Characterization

X-ray diffraction (XRD) patterns were obtained on a D8 Discover GADDS (Bruker AXS, Germany) powder diffractometer. Scanning electron microscopy (SEM) images were acquired with a JEOL-7600 field emission scanning electron microscope. Transmission electron microscopy (TEM), high-resolution transmission electron microscopy (HRTEM) and selected area electron diffraction (SAED) experiments were performed on a JEOL 2100 transmission electron microscopy at an accelerating voltage of 200 kV. Thermogravimetric analyses (TGA) were performed with a TGA Q500 at 700 °C with a heating rate of 10 °C min^{-1} in air. The Brunauer–Emmett–Teller (BET) test was determined via a Micromeritics Tristar II-3020 nitrogen adsorption apparatus. Pore size distribution plot was obtained by the Barrett–Joyner–Halenda (BJH) method.

2.3. Electrochemical measurements

To characterize electrochemical properties of the composites, a working electrode containing 60 wt.% active materials, 30 wt.% Super P, and 10 wt.% polyvinylidene fluoride was prepared. The electrochemical properties were measured with a standard CR2032 coin cell with lithium metal as the counter electrode, Celgard 2600 as the separator, and a solution of 1.0 M $LiPF_6$ in ethylene carbonate (EC)/dimethyl carbonate (DMC) (1:1 by volume) as the electrolyte. The cells were assembled in an argon-filled glove box and tested in the voltage range of 0.005 and 3.0 V (*vs.* Li^+/Li) with a Neware-CT3008 battery test system (Neware Technology Limited, Shenzhen, China). Cyclic voltammetry (CV) measurements were performed using an Autolab PGSTAT302N electrochemical workstation (Metrohm, Switzerland) at 0.1 mV/s in the voltage range of 0.005–3.0 V.

3. Results and discussion

Fig. 1 illustrates the synthesis route for the $ZnFe_2O_4$/graphene composites. In the first step, the two types of metal cations, i.e. Zn^{2+} and Fe^{2+}, in the precursor are hydrolyzed in the GO colloid suspension with the addition of ammonium

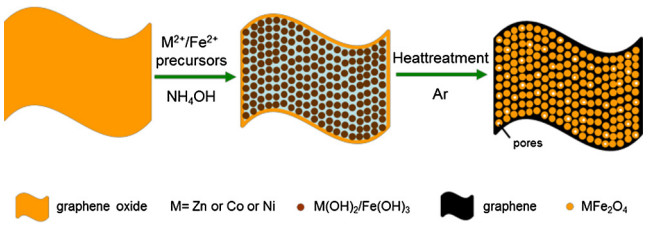

Fig. 1 – A schematic showing synthesis route for the mesoporous $ZnFe_2O_4$/graphene composites. (A color version of this figure can be viewed online.)

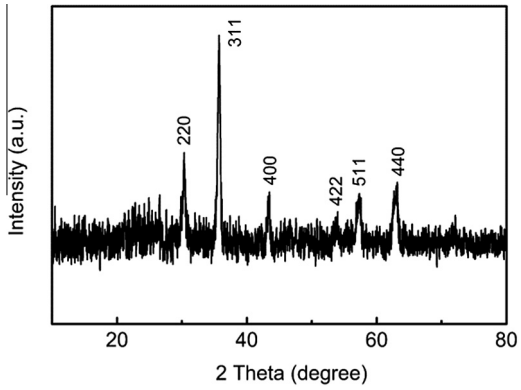

Fig. 2 – XRD pattern of the $ZnFe_2O_4$/graphene composites.

hydroxide. During the hydrolysis, Fe^{II} is rapidly oxidized into Fe^{III} in the presence of oxygen. Meanwhile, $Zn(OH)_2/Fe(OH)_3$ particles are anchored onto the surface of the GO nanosheets through the interaction of their hydroxyl groups with the GO. After this co-precipitation process, the $GO/Zn(OH)_2/Fe(OH)_3$ are calcinated in argon atmosphere. In this process, $Zn(OH)_2/Fe(OH)_3$ are decomposed, forming $ZnFe_2O_4$, and GO is converted into graphene. The graphene content in the composites is about 32 wt.% as determined by TGA.

Fig. 2 shows the XRD pattern of the obtained $ZnFe_2O_4$/graphene composites. The main diffraction peaks are at $2\theta = 29.9°$, 35.3° and 42.8°, which are corresponding to the reflections from the (220), (311) and (400) planes of the cubic phase of $ZnFe_2O_4$ (JCPDS No. 22-1012), respectively. No diffraction peaks corresponding to other phase or impurities are observed, indicating that highly pure $ZnFe_2O_4$ samples are obtained. SEM and TEM images for the $ZnFe_2O_4$/graphene composites are shown in Fig. 3. The low-magnification image in Fig. 3a shows that the $ZnFe_2O_4$/graphene composites are composed of irregularly shaped and wavy nanosheets with lateral dimensions of 10 μm. The high-magnification SEM image in Fig. 3b shows that the nanosheets are highly wrinkled with small $ZnFe_2O_4$ particles uniformly anchored on the surface. The typical $ZnFe_2O_4$ particle size is below 20 nm, which can be further confirmed by the TEM image in Fig. 3c. Different from the $ZnFe_2O_4$/graphene composites, the $ZnFe_2O_4$ nanoparticles are irregular in shape with the size of 20–30 nm, as shown in Fig. S1 in Supplement material. The SAED pattern of the $ZnFe_2O_4$/graphene composites (the inset in Fig. 3c) consists of intense reflection rings corresponding to the cubic structure of $ZnFe_2O_4$, which agrees well with the XRD pattern. The HRTEM image in Fig. 3d shows clear lattices with interplanar distance of 0.17 nm and 0.25 nm, which are consistent with the standard values for the (422) and (311) planes of the cubic structure of $ZnFe_2O_4$, respectively. It is worth mentioning that further increasing metal ion concentrations in the reaction system would lead to severe

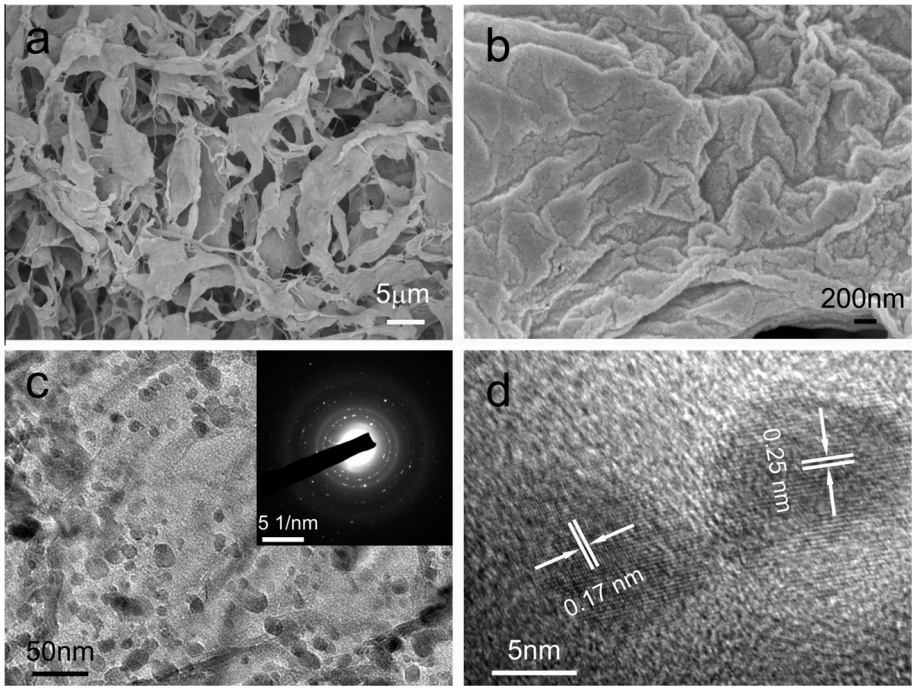

Fig. 3 – (a, b) SEM, (c) TEM and (d) HRTEM images of the $ZnFe_2O_4$/graphene composites; the inset in (c) is the corresponding SAED pattern.

aggregations of $ZnFe_2O_4$ nanoparticles on the graphene nanosheets (Fig. S2 in Supplement material). The small particle sizes of the anchored nanoparticles can greatly reduce the lithium-ion diffusion length in the nanoparticles and increase the accessible sites of the active material, leading to high rate capability and large capacity [30,31]. In addition, the anchoring structure would enable fast electron transport between the $ZnFe_2O_4$ nanoparticles and graphene sheets. This could help to reduce the inner resistance of LIBs and is beneficial for stabilizing the electronic and ionic conductivity, therefore resulting in higher specific capacities even at high discharge/charge current densities [32]. Moreover, the graphene nanosheets can also serve as a buffer layer for the volume expansion of the $ZnFe_2O_4$ nanoparticles during the lithiation/delithiation processes [33].

To examine the specific surface area and pore size distribution, N_2 adsorption–desorption isothermal measurements were performed. The results are shown in Fig. 4 and the insets are the corresponding BJH pore size distribution curves. It can be seen that the dominant pore sizes deduced from the BJH method are about 2.5, 9 and 45 nm, respectively, for the $ZnFe_2O_4$/graphene composites. The appearance of small pores with sizes of less than 10 nm are probably caused by the release of H_2O during the decomposition of hydroxides, while the large ones may be formed by loose packing of the nanosheets, *i.e.*, correspond to the interspaces between the $ZnFe_2O_4$/graphene nanosheets. The surface area of the composites estimated from the BET method is 282 m^2/g, which is much larger than the reported value for the $ZnFe_2O_4$/graphene composites made by hydrothermal process [18]. The large surface area of the $ZnFe_2O_4$/graphene composites may facilitate the electrolyte diffusion to active sites. In addition, the mesoporous morphology may accommodate the volume changes of $ZnFe_2O_4$ during Li-ion insertion/extraction, maintaining the structural integrity and hence enabling high capacity and cycling stability [34].

The electrochemical performances of the as-prepared mesoporous $ZnFe_2O_4$/graphene composites were evaluated with a standard CR2032 coin cell. Cyclic voltammetry (CV) was performed to identify the electrochemical reactions of the composites electrode, as shown in Fig. 5. Obviously, there is a substantial difference between the first cycle and subsequent cycles. In the first cathodic process, a peak at 1.51 V is observed, which can be generally attributed to the irreversible reaction with the electrolyte [35]. Besides, a small peak at around 0.88 V and a high-intensity peak at 0.72 V are also observed, which can be ascribed to the irreversible reaction of $ZnFe_2O_4$ with the metallic lithium to form Fe^0 and Zn^0 as well as the formation of Li–Zn alloys and Li_2O [36]. Moreover, a small peak at around 0.4 V may correspond to the lithium insertion onto the graphene sheets. Meanwhile, a broad peak at about 1.6 V is observed in the anodic process, which corresponds to the reversible oxidation of the metallic zinc and iron to Zn^{2+} and Fe^{3+} respectively [9]. In the subsequent cycles, both the peak current and the integrated area of the cathodic and anodic peaks are almost constant, indicating the capacity can be well maintained since 2nd cycle.

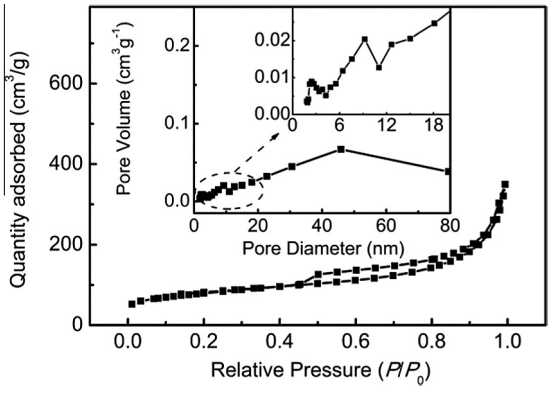

Fig. 4 – The nitrogen adsorption–desorption isotherms of the mesoporous $ZnFe_2O_4$/graphene composites; the insets are the corresponding BJH pore size distribution curves.

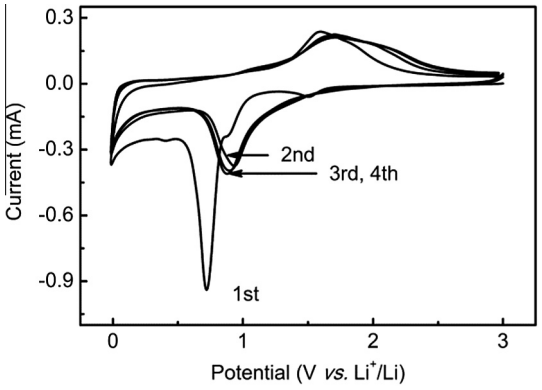

Fig. 5 – Cyclic voltammogram of the mesoporous $ZnFe_2O_4$/graphene composites.

Fig. 6a shows the discharge/charge curves of the mesoporous $ZnFe_2O_4$/graphene composites electrode in the voltage range of 0.005–3.0 V at a current density of 0.1 A/g. The electrode exhibits two discharge potential plateaus at around 1.48 V and 0.82 V in the first discharge process. The corresponding capacities for these two plateaus are ~37 mAh/g and 595 mAh/g, respectively, correlating to the consumption of about 0.5 and 8 mol of lithium per mole of $ZnFe_2O_4$, respectively. These results are well agree with the reported work [11], indicating the formation of $Li_{0.5}ZnFe_2O_4$ nanoparticles and the reduction of $ZnFe_2O_4$ to metallic iron and zinc accompanied by the formation of amorphous Li_2O, respectively. With the decreasing of the voltage to the discharge limit of 0.005 V, the specific capacity is extending to 1744 mAh/g, which is much higher than the theoretical capacity of $ZnFe_2O_4$. The ultrahigh first discharge capacity may be plausibly attributed to the lithium insertion to graphene as well as the irreversible reactions, such as the decomposition of electrolyte [37,38]. Apparently, the mesoporous $ZnFe_2O_4$/graphene composites electrode has a superior lithium storage capacity, though the Coulombic efficiency in the first cycle is only 67.7%. The discharge capacity is drastically decreased to 1223 mAh/g in the 2nd cycle. The large capacity loss between the 1st and the 2nd cycle is possibly associated with the formation of a solid electrolyte interface layer on the electrode surface during the first discharge process [39]. These results are consistent with the observation in the CV analysis mentioned earlier. Nevertheless, from the 2nd cycle onward, the

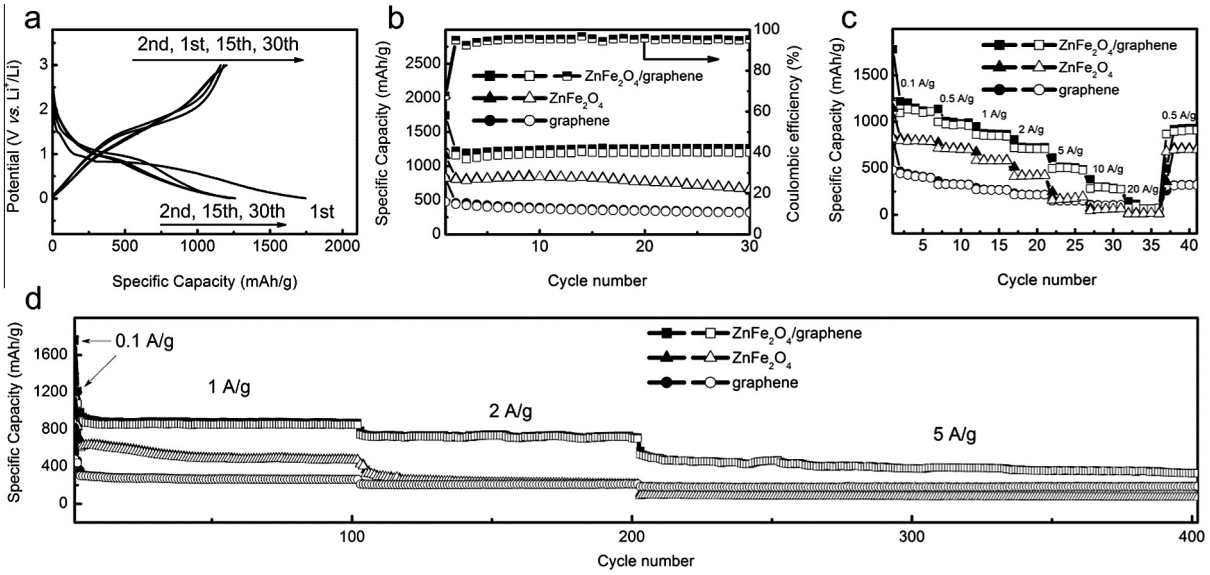

Fig. 6 – Electrochemical performances of the composites, $ZnFe_2O_4$ nanoparticles and graphene anodes: (a) galvanostatic charge/discharge profiles, (b) cycling performance and the Coulombic efficiency at 0.1 A/g, (c) rate performance and (d) rate cyclic capacities at different current densities.

composites electrode shows excellent cycling stability, and the Coulombic efficiency is increased to above 95% with increasing cycle number, as shown in Fig. 6b. Up to the 30th cycle, the reversible discharge/charge capacities can be maintained as high as 1259/1200 mAh/g. Similar discharge/charge curves are observed for the $ZnFe_2O_4$ nanoparticle electrode (Supplement material Fig. S3). The $ZnFe_2O_4$ nanoparticle electrode shows lower initial discharge/charge capacities of 1154/822 mAh/g and after 30 cycles the capacities are dropped to 677/660 mAh/g at the current density of 0.1 A/g. For the graphene electrode, the discharge/charge capacities at 0.1 A/g are only 330/318 mAh/g after 30 cycles.

To further demonstrate the electrochemical performance of the mesoporous $ZnFe_2O_4$/graphene composites anode, its rate capability was measured. It is striking to see that the composites anode shows fascinating rate performance, as shown in Fig. 6c. When the current density is increased from 0.1 to 20 A/g, the discharge/charge capacities are decreased regularly and kept stable at each current density. The reversible discharge capacities at 0.5, 1.0, 2.0, 5.0, 10 and 20 A/g are 990, 866, 726, 487, 275 and 90 mAh/g, respectively. Remarkably, a stable reversible discharge capacity of 931 mAh/g can be recovered when the current density returns to the 0.5 A/g. By contrast, the capacities of both the $ZnFe_2O_4$ nanoparticles and graphene decrease rapidly with the increasing current densities and the capacity values at 0.5, 1.0, 2.0, 5.0, 10 and 20 A/g are 709, 588, 425, 192, 69, 17 mAh/g for the $ZnFe_2O_4$ nanoparticles and 327, 269, 217, 154, 105, 61 mAh/g for the graphene, respectively. The superior cycling stability at high current densities is further demonstrated in Fig. 6d. The lithium cell using the mesoporous $ZnFe_2O_4$/graphene composites as the working electrode was also tested at 1.0, 2.0 and 5.0 A/g for 100, 100 and 200 cycles, respectively. The reversible discharge capacities can be maintained at 870 mAh/g at 1.0 A/g for 100 cycles and 713 mAh/g at 2.0 A/g for another 100 cycles. Obviously, the mesoporous $ZnFe_2O_4$/graphene composites anode shows excellent cycling stability at these two current densities and no obvious capacity fading is observed under each current density. When the current density is further increased to 5 A/g, the capacity gradually decays with increasing cycle number. Even though, a satisfactory reversible discharge capacity of 331 mAh/g, corresponding to 63% capacity retention, can be obtained after 200 cycles at 5 A/g. Generally, for the rate performance testing, it is necessary to use high Super P content to ensure good electric conductivity of the electrode and facilitate electron transport from the active materials to the current collector [34,40]. For the purpose of comparison, the electrochemical performances of the electrode composed of 80 wt.% $ZnFe_2O_4$/graphene composites, 10 wt.% Super P and 10 wt.% polyvinylidene fluoride were also tested, and the results are shown as Fig. S4 in Supplement material. Compared with the electrode with 30% Super P, the electrode composed of 10 wt.% Super P shows somewhat decreased capacities at different current densities, while it still exhibits fairly competitive electrochemical performances. Note that the specific capacities in our work are calculated based on the total mass of the $ZnFe_2O_4$/graphene composite. The performances shown here are still much superior than reported previously [7–11,17–19,27]. Moreover, after long-term high-rate cycling at 1.0, 2.0 and 5.0 A/g for 100, 100 and 200 cycles, the discharge capacities dropped to 473, 211, 68 mAh/g for the $ZnFe_2O_4$ nanoparticles and 264, 215, 188 mAh/g for the graphene electrode, respectively. Clearly, the $ZnFe_2O_4$/graphene composite possesses much better electrochemical properties than both the $ZnFe_2O_4$ nanoparticles and graphene. Although both the $ZnFe_2O_4$ nanoparticles and graphene could provide stable capacities at high rates, their specific capacity values are much lower than that of the $ZnFe_2O_4$/graphene composite because the $ZnFe_2O_4$ nanoparticles have relatively low electrical conductivity and poor interaction with the electrolyte owing to their strong aggregation tendency, whereas graphene may also

restack in processing to greatly reduce its specific surface area. It shows that by uniformly anchoring the $ZnFe_2O_4$ nanoparticles onto graphene, the synergetic effect between the anchored $ZnFe_2O_4$ nanoparticles and graphene can overcome the intrinsic limitations of the two components.

Compared with the electrochemical performance of various $ZnFe_2O_4$-based anodes reported in literatures [7–13,17–19,27], the mesoporous $ZnFe_2O_4$/graphene composites electrode in this work exhibits higher specific capacity, outstanding cycling stability, and excellent rate performance, which can be attributed to its unique structure and morphological features. On one hand, the graphene in the composites can serve as the conductive channels for the anchored $ZnFe_2O_4$ nanoparticles and accommodate the volume expansion as well as efficiently prevent the aggregation of $ZnFe_2O_4$ nanoparticles during the lithiation/delithiation processes. On the other hand, the small particle size of the anchored $ZnFe_2O_4$ nanoparticles guarantees the shorter Li-ion transport length and enhances the storage capacity which is the main characteristic of the nano-structured electrode material. More importantly, the mesopores in $ZnFe_2O_4$ nanoparticles can not only act as buffering spaces to accommodate volume changes during the discharging/charging processes but also enlarge the contact area between the electrode and electrolyte, providing more active sites for lithium ion insertion, especially at high rates. It can be concluded that the synergetic effect among the conducting graphene sheets, tightly anchored $ZnFe_2O_4$ nanoparticles and the presence of mesopores in the nanoparticles is responsible for the excellent electrochemical performance of the composites anode.

It is worth mentioning that the synthesis strategy used in this work is feasible for large-scale production, and it can also be used for preparing other graphene-based composites containing ferrites, such as cobalt ferrite and nickel ferrite, as shown in Fig 7. Obviously, the obtained ferrite/graphene composites also exhibit nanosheet morphology with the binary transition metal oxides anchoring on the graphene nanosheets. The sizes for these ferrites are about 15 and 50 nm for cobalt ferrite and nickel ferrite, respectively. The cubic structures for the obtained ferrites are verified by their XRD patterns. These results demonstrated the versatility of this facile two-step strategy for synthesis of various types of ferrite/graphene composites.

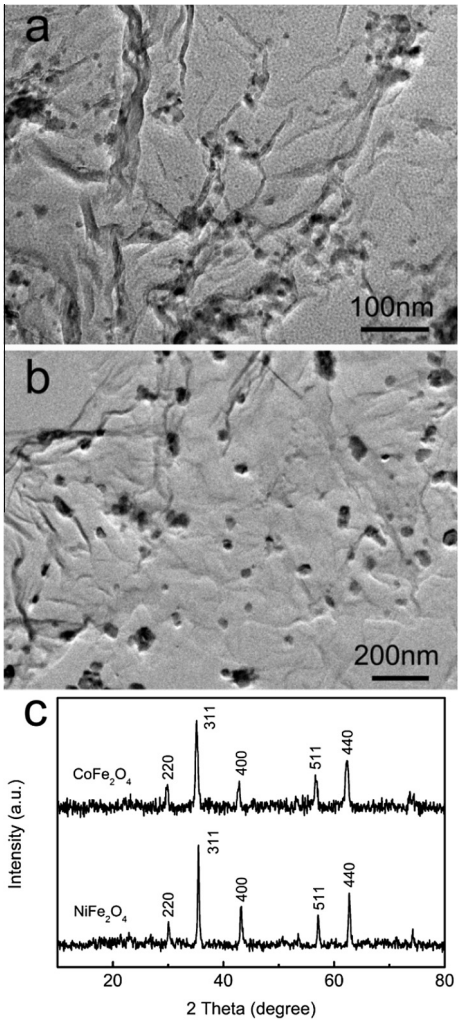

Fig. 7 – TEM images of (a) cobalt ferrite/graphene and (b) nickel ferrite/graphene composites; (c) XRD patterns of the composites.

4. Conclusions

We developed a facile two-step strategy for synthesizing mesoporous $ZnFe_2O_4$/graphene composites. In the composites prepared under optimized conditions, the $ZnFe_2O_4$ nanoparticles have sizes of less than 20 nm and are uniformly anchored on the graphene nanosheets. As an anode material for LIBs, the mesoporous $ZnFe_2O_4$/graphene composites deliver the first discharge/charge capacities as high as 1744/1181 mAh/g and its discharge/charge capacities are maintained at 1259/1200 mAh/g after 30 cycles at 0.1 A/g. The anode also shows excellent rate capability and cycling stability, exhibiting stable reversible discharge specific capacities of 870 mAh/g at 1.0 A/g for 100 cycles and 713 mAh/g at 2.0 A/g for another 100 cycles. The superior electrochemical performance of the mesoporous $ZnFe_2O_4$/graphene composites could be ascribed to the synergetic effect among the conducting graphene sheets, tightly anchored $ZnFe_2O_4$ nanoparticles and the presence of mesopores in the particles. In addition, the synthesis strategy can be used as a generic route for synthesizing other graphene/binary transitional metal oxide composites for LIBs or other applications.

Appendix A. Supplementary data

Supplementary data associated with this article can be found, in the online version, at http://dx.doi.org/10.1016/j.carbon.2014.08.007.

REFERENCES

[1] Armand M, Tarascon JM. Building better batteries. Nature 2008;451(7179):652–7.
[2] Jiang J, Li YY, Liu JP, Huang XT, Yuan CZ, Lou XW. Recent advances in metal oxide-based electrode architecture design

for electrochemical energy storage. Adv Mater 2012;24(38):5166–80.
[3] Reddy MV, Rao GVS, Chowdari BVR. Metal oxides and oxysalts as anode materials for li ion batteries. Chem Rev 2013;113(7):5364–457.
[4] Fan Y, Zhang Q, Xiao QZ, Wang XH, Huang K. High performance lithium ion battery anodes based on carbon nanotube-silicon core-shell nanowires with controlled morphology. Carbon 2013;59:264–9.
[5] Liu C, Li F, Ma LP, Cheng HM. Advanced materials for energy storage. Adv Mater 2010;22(8):E28–62.
[6] Li Y, Guo BK, Ji LW, Lin Z, Xu GJ, Liang Y, et al. Structure control and performance improvement of carbon nanofibers containing a dispersion of silicon nanoparticles for energy storage. Carbon 2013;51:185–94.
[7] Sharma Y, Sharma N, Rao GVS, Chowdari BVR. Li-storage and cyclability of urea combustion derived $ZnFe_2O_4$ as anode for Li-ion batteries. Electrochim Acta 2008;53(5):2380–5.
[8] Xu HY, Chen XL, Chen L, Li LE, Xu LQ, Yang J, et al. A comparative study of nanoparticles and nanospheres $ZnFe_2O_4$ as anode material for lithium ion batteries. Int J Electrochem Sci 2012;7(9):7976–83.
[9] Guo XW, Lu X, Fang XP, Mao Y, Wang ZX, Chen LQ, et al. Lithium storage in hollow spherical $ZnFe_2O_4$ as anode materials for lithium ion batteries. Electrochem Commun 2010;12(6):847–50.
[10] Teh PF, Sharma Y, Pramana SS, Srinivasan M. Nanoweb anodes composed of one-dimensional, high aspect ratio, size tunable electrospun $ZnFe_2O_4$ nanofibers for lithium ion batteries. J Mater Chem 2011;21(38):14999–5008.
[11] Sui JH, Zhang C, Hong D, Li J, Cheng Q, Li ZG, et al. Facile synthesis of MWCNT-$ZnFe_2O_4$ nanocomposites as anode materials for lithium ion batteries. J Mater Chem 2012;22(27):13674–81.
[12] Bresser D, Paillard E, Kloepsch R, Krueger S, Fiedler M, Schmitz R, et al. Carbon coated $ZnFe_2O_4$ nanoparticles for advanced lithium-ion anodes. Adv Energy Mater 2013;3(4):513–23.
[13] Mueller F, Bresser D, Paillard E, Winter M, Passerini S. Influence of the carbonaceous conductive network on the electrochemical performance of $ZnFe_2O_4$ nanoparticles. J Power Sources 2013;236:87–94.
[14] Huang X, Zeng ZY, Fan ZX, Liu JQ, Zhang H. Graphene-based electrodes. Adv Mater 2012;24(45):5979–6004.
[15] Xu CH, Xu BH, Gu Y, Xiong ZG, Sun J, Zhao XS. Graphene-based electrodes for electrochemical energy storage. Energy Environ Sci 2013;6(5):1388–414.
[16] Mahmood N, Zhang CZ, Yin H, Hou YL. Graphene-based nanocomposites for energy storage and conversion in lithium batteries, supercapacitors and fuel cells. J Mater Chem A 2014;2(1):15–32.
[17] Song WT, Xie J, Liu SY, Cao GS, Zhu TJ, Zhao XB. Self-assembly of a $ZnFe_2O_4$/graphene hybrid and its application as a high-performance anode material for Li-ion batteries. New J Chem 2012;36(11):2236–41.
[18] Xia H, Qian YY, Fu YS, Wang X. Graphene anchored with $ZnFe_2O_4$ nanoparticles as a high-capacity anode material for lithium-ion batteries. Solid State Sci 2013;17:67–71.
[19] Chen XL, Cheng B, Xu HY, Yang J, Qian YT. Porous $ZnFe_2O_4$ nanospheres grown on graphene nanosheets as a superior anode material for lithium ion batteries. Chem Lett 2012;41(6):639–41.
[20] Fu YS, Wang X. Magnetically separable $ZnFe_2O_4$-graphene catalyst and its high photocatalytic performance under visible light irradiation. Ind Eng Chem Res 2011;50(12):7210–8.
[21] Lu DB, Zhang Y, Lin SX, Wang LT, Wang CM. Synthesis of magnetic $ZnFe_2O_4$/graphene composite and its application in photocatalytic degradation of dyes. J Alloy Compd 2013;579:336–42.
[22] Fei P, Zhong M, Lei ZQ, Su BT. One-pot solvothermal synthesized enhanced magnetic zinc ferrite-reduced graphene oxide composite material as adsorbent for methylene blue removal. Mater Lett 2013;108:72–4.
[23] Vu A, Qian YQ, Stein A. Porous electrode materials for lithium-ion batteries – how to prepare them and what makes them special. Adv Energy Mater 2012;2(9):1056–85.
[24] Li Y, Fu ZY, Su BL. Hierarchically structured porous materials for energy conversion and storage. Adv Funct Mater 2012;22(22):4634–67.
[25] Wang M, Ai ZH, Zhang LZ. Generalized preparation of porous nanocrystalline $ZnFe_2O_4$ superstructures from zinc ferrioxalate precursor and its superparamagnetic property. J Phys Chem C 2008;112(34):13163–70.
[26] Meng WQ, Li F, Evans DG, Duan X. Photocatalytic activity of highly porous zinc ferrite prepared from a zinc-iron(III)-sulfate layered double hydroxide precursor. J Porous Mater 2004;11(2):97–105.
[27] Woo MA, Kim TW, Kim IY, Hwang SJ. Synthesis and lithium electrode application of ZnO-$ZnFe_2O_4$ nanocomposites and porously assembled $ZnFe_2O_4$ nanoparticles. Solid State Ionics 2011;182(1):91–7.
[28] Hummers WS, Offeman RE. Preparation of graphitic oxide. J Am Chem Soc 1958;80(6):1339.
[29] Zhou XF, Liu ZP. A scalable, solution-phase processing route to graphene oxide and graphene ultralarge sheets. Chem Commun 2010;46(15):2611–3.
[30] Xin X, Zhou XF, Wu JH, Yao XY, Liu ZP. Scalable synthesis of TiO_2/graphene nanostructured composite with high-rate performance for lithium ion batteries. ACS Nano 2012;6(12):11035–43.
[31] Wu ZS, Ren WC, Wen L, Gao LB, Zhao JP, Chen ZP, et al. Graphene anchored with Co_3O_4 nanoparticles as anode of lithium ion batteries with enhanced reversible capacity and cyclic performance. ACS Nano 2010;4(6):3187–94.
[32] Jiang CH, Hosono E, Zhou HS. Nanomaterials for lithium ion batteries. Nano Today 2006;1(4):28–33.
[33] Paek SM, Yoo E, Honma I. Enhanced cyclic performance and lithium storage capacity of SnO_2/graphene nanoporous electrodes with three-dimensionally delaminated flexible structure. Nano Lett 2009;9(1):72–5.
[34] Yao XY, Tang CL, Yuan GX, Cui P, Xu XX, Liu ZP. Porous hematite (alpha-Fe_2O_3) nanorods as an anode material with enhanced rate capability in lithium-ion batteries. Electrochem Commun 2011;13(12):1439–42.
[35] He Y, Huang L, Cai JS, Zheng XM, Sun SG. Structure and electrochemical performance of nanostructured Fe_3O_4/carbon nanotube composites as anodes for lithium ion batteries. Electrochim Acta 2010;55(3):1140–4.
[36] Ding Y, Yang YF, Shao HX. High capacity $ZnFe_2O_4$ anode material for lithium ion batteries. Electrochim Acta 2011;56(25):9433–8.
[37] Nam KT, Kim DW, Yoo PJ, Chiang CY, Meethong N, Hammond PT, et al. Virus-enabled synthesis and assembly of nanowires for lithium ion battery electrodes. Science 2006;312(5775):885–8.
[38] Lou XW, Deng D, Lee JY, Feng J, Archer LA. Self-supported formation of needlelike Co_3O_4 nanotubes and their application as lithium-ion battery electrodes. Adv Mater 2008;20(2):258–62.
[39] Lu L, Wang JZ, Zhu XB, Gao XW, Liu HK. High capacity and high rate capability of nanostructured $CuFeO_2$ anode materials for lithium-ion batteries. J Power Sources 2011;196(16):7025–9.
[40] Kang B, Ceder G. Battery materials for ultrafast charging and discharging. Nature 2009;458(7235):190–3.